Published in final edited form as:
Neuron. 2007 April 5; 54(1): 137–152.

The Emergence of Contrast-Invariant Orientation Tuning in Simple Cells of Cat Visual Cortex

Ian M. Finn[*], **Nicholas J. Priebe**[*], and **David Ferster**
Department of Neurobiology and Physiology, Northwestern University, 2205 Tech Drive, Evanston, IL 60208, USA.

Abstract

Simple cells in primary visual cortex exhibit contrast-invariant orientation tuning, in seeming contradiction to feed-forward models relying on lateral geniculate nucleus (LGN) input alone. Contrast invariance has therefore been thought to depend on the presence of intracortical lateral inhibition. *In vivo* intracellular recordings instead suggest that contrast invariance can be explained by three properties of the excitatory pathway. 1) Depolarizations evoked by orthogonal stimuli are determined by the amount of excitation a cell receives from the LGN, relative to the excitation it receives from other cortical cells. 2) Depolarizations evoked by preferred stimuli saturate at lower contrasts than the spike output of LGN relay cells. 3) Visual stimuli evoke contrast-dependent changes in trial-to-trial variability, which lead to contrast-dependent changes in the relationship between membrane potential and spike rate. Thus, high-contrast, orthogonally-oriented stimuli that evoke significant depolarizations evoke few spikes. Together these mechanisms, without lateral inhibition, can account for contrast-invariant stimulus selectivity.

Keywords

primary visual cortex; spike threshold nonlinearity; intracellular recording; lateral geniculate nucleus; contrast invariance; trial-to-trial variability; orientation selectivity

Introduction

In the classical view of sensory processing, generalized from Hartline's description of the limulus retina (Hartline, 1949), excitatory connections establish a bias in the selectivity of sensory neurons; lateral inhibition is then required to refine and sharpen this bias into the exquisitely selective responses sensory neurons often exhibit. According to this view, in the visual cortex excitatory, feed-forward connections from the lateral geniculate nucleus (LGN) establish the broad outlines of cortical receptive fields, including orientation bias and subfield organization (DeAngelis et al., 1993b;Hubel and Wiesel, 1962;Movshon et al., 1978;Reid and Alonso, 1995), but these connections seem, on their own, to be unable to explain more subtle aspects of cortical responses, such as the sharpness of orientation tuning, cross-orientation suppression, and contrast invariance of orientation tuning. Lateral inhibition is thought to remedy the failures of the feed-forward model, either in the form of synaptic inhibition among neurons with different orientation tuning (Heeger, 1992;Lauritzen and Miller,

Proofs and Correspondence to: David Ferster, Department of Neurobiology and Physiology, Northwestern University, 2205 Tech Drive, Evanston, IL 60208, Voice: (847) 491-4137, Fax: (847) 491-5211, E-mail: ferster@northwestern.edu
[*]Equal contribution

2003;McLaughlin et al., 2003;Somers et al., 1995;Sompolinsky et al., 1990;Troyer et al., 1998), or inhibition from neurons that are untuned for orientation (Hirsch et al., 2003;Lauritzen and Miller, 2003).

Despite the computational power of lateral inhibition, direct evidence that it shapes orientation selectivity in the cortex is equivocal (Anderson et al., 2000b;Borg-Graham et al., 1998;Ferster, 1986;Martinez et al., 2002). As an alternative to lateral inhibition, the failures of the feed-forward model can in part be accounted for by the inclusion of experimentally demonstrated nonlinear properties of the visual pathway, properties such as threshold, contrast saturation, synaptic depression and spike-rate rectification (Carandini and Ferster, 2000;Freeman et al., 2002;Priebe and Ferster, 2006). Unlike orientation-specific inhibition, these nonlinearities (like untuned inhibition) are feature-blind: They operate independently of stimulus orientation, direction or size, but instead filter all signals as a function of stimulus strength (contrast) or response amplitude (spike rate).

This latter approach of incorporating non-linearities into the feed-forward model has been used to explain several fundamental aspects of simple-cell responses. The non-linearity of spike threshold can account for why simple cells' spike responses have sharper orientation tuning (Carandini and Ferster, 2000;Volgushev et al., 2000) and higher direction selectivity (Jagadeesh et al., 1997;Priebe and Ferster, 2005) than predictions derived from receptive field maps (DeAngelis et al., 1993b;Tolhurst and Heeger, 1997). Contrast saturation and spike-rate rectification of relay cells in the LGN can account for a large measure of cross-orientation suppression (Li et al., 2006;Priebe and Ferster, 2006).

One observation that remains difficult to reconcile with a purely feed-forward model is contrast invariance of orientation tuning (Alitto and Usrey, 2004;Skottun et al., 1987). As contrast increases, relay cell input to simple cells should increase at all orientations, including the orientation orthogonal to the preferred (Ferster and Miller, 2000;Troyer et al., 1998). Thus at higher contrasts, stimuli further and further from the preferred orientation, and ultimately at all orientations, should evoke suprathreshold depolarizations and elicit spikes, leading to a broadening of orientation tuning (the so-called iceberg effect). And yet, most simple cells respond with few or no spikes at the orthogonal orientation, and orientation tuning is largely contrast invariant (Alitto and Usrey, 2004;Anderson et al., 2000c;Ferster and Miller, 2000;Skottun et al., 1987).

In models dependent on lateral inhibition, inhibitory input counteracts the excitatory relay-cell input that occurs at the null orientation, thus preventing a contrast-dependent broadening in orientation tuning. To ascertain whether tuned inhibition is required to refine cortical orientation tuning in this way, we recorded intracellularly from a large population of simple cells. We compared the contrast dependence of orientation tuning – both for membrane potential and spike rate – to the predictions of a feed-forward, excitation-only model based on the recorded behavior of geniculate relay cells. Consistent with the feed-forward model, many simple cells depolarized significantly in response to stimuli orthogonal to the preferred orientation. The amplitude of this depolarization was directly related to the fraction of direct synaptic input each cell received from the LGN. Thus, intracortical inhibition is not required to set the amplitude of the depolarization evoked by null stimuli. We also found that membrane potential responses to preferred stimuli saturated at lower contrasts than did spike responses of relay cells. These two properties had a significant effect on the contrast dependence of orientation tuning: tuning width did change with contrast, but less so than was expected from the feed-forward model.

Contrast-dependence of orientation tuning width was further reduced in the spike responses of simple cells by two features of the transformation between membrane potential and spike rate.

The first is the expansive nonlinearity of threshold, previously described as a power-law (Hansel and van Vreeswijk, 2002;Miller and Troyer, 2002;Priebe et al., 2004), which amplifies small differences in membrane potential into large differences in spike rate. Second, we find that the gain of the membrane-potential-to-spike-rate transformation is contrast dependent, falling with increasing contrast as a result of a concomitant fall in the trial-to-trial variability of responses. This change in gain helps prevent high-contrast stimuli of the non-preferred orientation from evoking spike responses, and consequently helps to generate contrast invariance in the spike responses of simple cells.

Our data thus support a model of orientation tuning in the visual cortex that operates without the need for lateral inhibition. Complex properties such as contrast-invariance can instead arise from the feed-forward pathway and its inherent nonlinearities.

Results

Contrast dependence of orientation tuning in a simple feed-forward model

We begin by examining the properties of a purely linear feed-forward model in which we have expressly omitted inhibition of any type, even push-pull inhibition at the preferred orientation (Ferster, 1988;Hirsch et al., 1998). Our purpose here is to explore how well a purely excitatory feed-forward model can or cannot account for contrast invariance of orientation tuning in simple cells. The extent to which the model fails or succeeds would then lead to conclusions about how inhibition might or might not contribute to invariance. The comparison between model and data serves to highlight quantitatively where the recorded behavior of simple cells diverges from strict linearity, and what mechanisms might underlie this divergence.

Unlike in previous models (Somers et al., 1995;Tao et al., 2004;Troyer et al., 1998), we make no assumptions about the properties of geniculate relay cells, such as spontaneous activity, modulation amplitude, rectification, or contrast saturation. Instead, we constructed the model from the measured responses of geniculate X cells, recorded under the same conditions we used when recording from cortical simple cells. As a result, the model has only one free parameter -- the aspect ratio of the simple cell subfields -- which affects the width of orientation tuning, but has little effect on the response attribute we examine here: the change of tuning width with contrast.

To construct the model, we recorded extracellularly from 16 ON- and OFF-center geniculate X cells while presenting drifting gratings at 8 different contrasts (0, 4, 8, 12, 16, 20, 32, and 64%)(Priebe and Ferster, 2006). We then averaged the responses of all 16 cells at each contrast (after shifting the response phases to be synchronous) and assigned these average responses to a template relay cell. The responses of 8 template ON-center relay cells with vertically offset receptive fields were summed to create the input to the simple cell from its ON subfield. Eight additional OFF-center relay cells were used to create the input from the OFF subfield (Fig. 1A, top; only 4 relay cells of each type are shown). The total relay-cell input was scaled so that an optimal, high-contrast stimulus evoked a 15-mV peak depolarization in the simple cell, similar to many recorded simple cells.

As in any feed-forward model, the alignment of the relay cell receptive fields makes the relative temporal phases of their responses dependent on the orientation of the stimulus: For the orientation orthogonal to the axis of displacement (null orientation), the relay cells respond asynchronously (Fig. 1B, 1st column, red and blue histograms). As a result, the null-oriented stimulus generates a rise in the mean potential, but no modulation component (Fig. 1A, 1st column, black histogram). For the preferred orientation, the ON and OFF relay cells respond synchronously (note that the red and blue ON- and OFF-center cell responses are therefore superimposed in Fig. 1B, 2nd column to make the violet histograms). As a result, the preferred

stimulus generates a large modulation (F1 component) in the simple cell's membrane potential (Fig. 1B, 1st column, black histogram), which rides on top of a rise in mean potential (DC component). At lower contrasts, the responses are similarly shaped but with smaller amplitudes (Fig. 1A and B, 3rd and 4th columns).

At any given contrast, the modulation (F1) component of the relay cell input is tuned for orientation with a Gaussian-shaped tuning curve (Fig. 1C, left). The width of the tuning curve (σ = 32 degrees in Equation 3; see Methods) is dependent only on the aspect ratio of the subfields, with higher aspect ratios giving rise to narrower tuning (DeAngelis et al., 1993a;Lampl et al., 2001;Palmer and Jones, 1984). The aspect ratio we have chosen, 2.5:1, is the smallest for which the amplitude of the F1 component falls to 0 at an orientation of 90 degrees.

The mean (DC) component of the relay cell input – the total input to the simple cell averaged over one cycle of the grating – is independent of aspect ratio and is untuned for orientation (Fig. 1C, right) because the relay cells themselves are insensitive to orientation. Note that the DC component originates from rectification of the firing rate of relay cells. Visual stimuli modulate a relay cell's firing rate around its relatively low spontaneous rate, and so while the peak rate can increase more or less without bound, the trough is clipped at 0 spikes per second. As a result, for all but the lowest contrasts, the mean firing rate of relay cells increases with contrast (Troyer et al., 1998).

One measure we use below for quantifying the contrast invariance of orientation tuning is the peak of the simple cell response during a grating cycle, which is well approximated by summing the DC and F1 components. The tuning of the peak response therefore forms a roughly Gaussian shaped curve (the F1 component) riding on top of an offset from rest (the DC component), both of which increase with contrast (Fig. 1D).

To derive the spiking responses of the model simple cell, we first applied a threshold-linear transformation to the tuning curves of peak membrane potential (Fig. 1E and F). This transformation results in a strong dependence of tuning width on contrast, with a significant broadening as contrast increase. At the lowest contrasts the responses nearly disappear entirely; at the highest contrasts, spikes are evoked at all orientations. This broadening is the so-called iceberg effect of threshold and is in direct contradiction to the behavior of real simple cells: Few real simple cells respond with spikes to stimuli of the null orientation at any contrast, and the spike-rate responses of real simple cells show minimal contrast-dependent changes in orientation tuning width (Alitto and Usrey, 2004;Anderson et al., 2000c;Skottun et al., 1987).

A second, more realistic representation of the V_m-to-spike-rate transformation is a power law (Hansel and van Vreeswijk, 2002;Miller and Troyer, 2002;Priebe et al., 2004):

$$R(V_m) = k\left\lfloor \overline{V}_m - V_{rest} \right\rfloor_+^p \quad (1)$$

where R is spike rate, $\overline{V}_m$ is trial-averaged membrane potential, V_{rest} is resting membrane potential, and the subscript, +, indicates rectification (R=0 for $V_m < V_{rest}$). The power law accounts for the effect of trial-to-trial variability by smoothing the threshold-linear relationship between mean membrane potential and mean spike rate (Anderson et al., 2000c). That is, even when a stimulus is weak and its mean response amplitude is far below physiological threshold, on a few trials the stimulus can carry the membrane potential above threshold and evoke spikes, leading to a small, but non-zero mean spike rate. In other words, variability smoothes (but does not completely linearize) the relationship between membrane potential and spike rate. We assign no theoretical significance to the power law but use it merely as a mathematical

convenience to account for trial-to-trial variability. Other equivalent mathematical approaches are possible.

Smoothing the relationship between membrane potential and spike rate mitigates some of the effects of contrast on orientation selectivity, as shown in predictions of spike rate based on the power law (Fig. 1G–I). The widths of the resulting orientation tuning curves are much less dependent on contrast than those derived from the threshold-linear transformation. When normalized (Fig. 1H, right), the curves are closely superimposed. When displayed with an expanded vertical scale (Fig. 1I), however, the tuning curves reveal significant deviations from experimental results. First, a low-contrast stimulus of the preferred orientation evokes a smaller spike response than a high-contrast stimulus of the null orientation (Fig. 1I, left, red circles). Second, the curves still broaden visibly with increasing contrast (Fig. 1I, right).

The response to high-contrast stimuli at the null orientation

In contrast to Figure 1D and I, for most simple cells we have studied intracellularly to date, high-contrast stimuli at the null-orientation evoke small membrane depolarizations, and very few (if any) spikes, relative to the preferred low-contrast response (Anderson et al., 2000b;Anderson et al., 2000c;Carandini and Ferster, 2000). The orientation tuning curves for membrane potential in these cells look more like what is illustrated in Fig. 1J–L. Here, the untuned DC components of the responses have been set to 0. Membrane potential responses are therefore perfectly contrast invariant (Fig. 1K), and the power law preserves invariance in the spike responses while narrowing the tuning width at all contrasts equally (Fig. 1L) (Anderson et al., 2000a;Hansel and van Vreeswijk, 2002;Miller, 1994). That the null response expected from the feed-forward model has apparently been suppressed in most cells has been attributed to cross-orientation inhibition or untuned inhibition (Ferster and Miller, 2000;Sompolinsky and Shapley, 1997).

To investigate whether the depolarization expected in response to null-oriented, high-contrast stimuli is consistently absent, we recorded intracellularly from 127 simple cells. Overall we found a wide range of behaviors, with some cells showing little depolarization at the null orientation (Fig. 2A), others showing moderate depolarization (B), and still others showing large depolarization (C). The model predicts that for any contrast the mean depolarization evoked by the null oriented grating (DC_N) should equal the mean depolarization evoked by the preferred orientation (DC_P). Within the recorded population, a significant number of cells echoed previous reports in showing a much smaller DC_N than DC_P (Fig. 2D, points below the unity line). Many points in Fig. 2D did, however, fall on or near the unity line as predicted by the feed-forward model of Figure 1. In only a small number of cells did the null-oriented stimulus cause a significant hyperpolarization of the membrane potential (Monier et al., 2003). The median DC_N/DC_P ratio for this population was 0.43 (Fig. 2E).

The feed-forward model is based on the assumption that simple cells receive all of their excitatory input from geniculate relay cells. In reality, each simple cell receives a different proportion of its excitatory input from the LGN, with the remainder coming from other cortical cells (Chung and Ferster, 1998). If intracortical connections are formed among cells with similar preferred orientation, simple cells with a large fraction of cortical excitatory input should exhibit small DC_N/DC_P ratios because cortical cells respond little to null-oriented stimuli (Chung and Ferster, 1998). Conversely, simple cells that receive the bulk of their input from the LGN should exhibit large DC_N/DC_P ratios. We tested this expectation for 19 cells, measuring the relationship between DC_N/DC_P and the fraction of excitatory input the cell received from the LGN (%LGN Input).

The %LGN Input was measured for each simple cell by suppressing the responses of cortical neurons with electrical stimulation (Chung and Ferster, 1998). We presented a 20-ms flash of

a high-contrast grating of optimal size, spatial frequency, spatial phase and orientation, with and without paired electrical stimulation of the nearby cortex. The electrical stimulus evokes a large IPSP in every nearby cortical cell and prevents spiking in response to the visual stimulus. To prevent the electrical stimulus from antidromically activating geniculate relay cells (Chung and Ferster, 1998), the stimulating electrode was inserted no deeper than 400 μm below the cortical surface, and stimulus amplitudes were kept in the range of 0.25–0.45mA (200μs duration, , electrode negative < 1mm distant from recording electrode). The response to paired electrical and visual stimulation (Fig. 3A–C, brown traces; the response to electrical stimulation alone has been subtracted off) is therefore dominated by direct, monosynaptic LGN input. The %LGN Input is taken to be the amplitude of the paired response divided by the amplitude of the response to the flashed grating alone (Fig. 3A–C, top, black traces).

The DC_N/DC_P ratio was well correlated with the %LGN Input. The DC_N/DC_P ratios for the three cells of Fig. 3A–C were 0, 0.45, and 0.85; their %LGN Input was 4%, 44%, and 86%. A scatterplot of DC_N/DC_P against %LGN Input for the 19 cells showed a strong correlation (Fig. 3D, $R^2 = 0.79$, slope = 0.76, Y-intercept = 0.13), with most of the points lying close to the unity line. A broad range of %LGN Input received by each cell can thus account for why the DC component of the grating response was often orientation tuned, i.e., why the average depolarization evoked by null-oriented stimuli in Fig. 2D and E was often smaller than the average depolarization evoked by preferred stimuli. This result is diagramed in the cartoon of Fig. 3E. The orientation tuning of relay cell responses, and the resulting input to a simple cell, is shown at the far left. In the center is depicted the input to a cell that receives 50% of its excitatory input from the LGN (top) and 50% from other cortical cells (bottom). These sum to produce the input pictured on the right. Thus, replacing some geniculate excitation with cortical excitation (from cells with similar preferred orientations) reduces the response at the null orientation while leaving the response at the preferred orientation unchanged.

We note parenthetically that shunting inhibition evoked by the shock stimulus, in addition to inactivation of cortical inputs, could in theory reduce the size of the response to the flash, making the %LGN Input appear to be smaller than it actually was. This is likely not the case. 1) Shock-evoked conductance changes (Anderson et al., 2000b) are not likely to be that much larger than changes evoked by the flash alone(Hirsch et al., 1998). 2) %LGN Input near 100% would likely not be observed. 3) The average %LGN Input observed here is comparable to that measured in cortical cooling experiments (Ferster et al., 1996), which are not subject to shunting effects. We therefore take the shock-induced reduction in flash response as a reasonable approximation of geniculate input.

Contrast saturation at the preferred orientation

The feed-forward model of Fig. 1 makes specific predictions about the contrast dependence of membrane potential responses in simple cells. Specifically, membrane potential should saturate with contrast in the same way that geniculate relay cell spike responses do. We therefore compared the contrast saturation of membrane potential responses in 46 simple cells with the spike responses of 45 geniculate X cells. The X cell in Fig. 4A and B reached half-maximal response amplitude (C_{50}) at 29% contrast. Overall, LGN cells had C_{50}'s between 4% and 35% contrast, with a median C_{50} of 15.9% (Fig. 4C). Simple cell membrane potential responses differed significantly from LGN cells. The membrane potential responses of the cell in Fig. 4D and E reached nearly complete saturation at 16% contrast. The median C_{50} for simple cells was 7.6% (Fig. 4F).

Possible sources for the early simple cell contrast saturation include depolarization-induced reductions in driving force on synaptic currents, and activity-dependent synaptic depression (Carandini et al., 2002;Kayser et al., 2001), which can reach nearly 50% in geniculocortical synapses (Bannister et al., 2002;Boudreau and Ferster, 2005) and 80–90% in corticocortical

synapses (Abbott et al., 1997;Stratford et al., 1996;Tsodyks and Markram, 1997). While not explicitly tested here, both of these potential mechanisms would affect off-orientation responses similarly to the preferred orientation response.

The early contrast saturation of membrane potential at the preferred orientation has important consequences for contrast invariance. The contrast can be lowered far more than would be expected from the feed-forward model before the synaptic input falls significantly. In other words, real tuning curves – both for membrane potential and spike rate – change much less with contrast than is shown in Fig. 1D (Fig. 4G).

Comparison of responses to high-contrast null stimuli and low-contrast preferred stimuli

The principle difficulty for contrast invariance raised by the model of Fig. 1 is the relationship between responses to high-contrast, null-oriented stimuli and low-contrast, preferred stimuli: The former are predicted to be larger than the latter (Fig. 1D, red dots), whereas in real simple cells – at least for spiking responses – the opposite is true (Fig. 5). In Figs. 2–4, we illustrated two features of simple-cell input that tend to mitigate this problem – one, a smaller depolarization at the null orientation than predicted, and two, earlier than expected contrast saturation. As a result, for most cells, the ratio of the null response at high-contrast (64%) to the preferred response at low-contrast (4%, 8% or 12%; points in Fig. 5A) was lower than expected from the feed-forward model (lines of corresponding color). Nevertheless, the problem remains as to why the depolarizations, though of reduced amplitude, evoked almost no spikes. Low-contrast preferred stimuli evoked depolarizations on average only about twice the size of those evoked by the null orientation (Fig. 5A), and yet they evoked vastly more spiking (Fig. 5B). In several simple cells of Fig. 5A, the membrane potential responses to high-contrast null stimuli and low-contrast preferred stimuli were nearly equal, and yet there are no cells in Fig. 5B with comparable spiking responses to the two stimuli. A single expansive nonlinearity is insufficient to account for this differential amplification, thus suggesting that the transformation between membrane potential and spike rate depends on contrast.

The effects of contrast on the transformation between membrane potential and spike rate

Spike rate is plotted against membrane potential separately for high- and low-contrast stimuli in Fig. 6A. Here, the cycle-averaged responses of all orientations were divided into 30-ms epochs, and mean spike rate was plotted against mean membrane potential for each epoch. As hinted at in Fig. 5, a given mean depolarization at high contrast evoked fewer spikes than the same depolarization at low contrast. We quantified this trend by comparing spike rate responses for stimuli of high and low contrast that evoked the same mean membrane potential (Fig. 6B; 2-mV bins for membrane potential). Judging by the average slope of the plot in Fig. 6B, on average a high-contrast stimulus evoked 62% of the spikes evoked by a low-contrast stimulus that gave rise to the same mean depolarization. Across 39 cells, this slope ranged from 0.01 to 1.2, with a median value of 0.49. Thus, stimulus contrast changed the gain of the membrane-potential-to-spike-rate transformation by a factor of about 2.

To understand the source of this change in gain between high and low contrast, it is important to note that the relationship plotted in Fig. 6A is the *mean* membrane potential against *mean* spike rate, averaged across stimulus trials. As shown previously, this relationship approximates a power law (Eq. 1), or a threshold-linear curve smoothed by trial-to-trial variability (smooth curves in Fig. 6A). The parameters of the power law are mainly determined by (1) the resting membrane potential of the cell, (2) the cell's threshold, and (3) the amount of noise or trial-to-trial variability in the membrane potential responses (Carandini, 2004;Chance et al., 2002;Hansel and van Vreeswijk, 2002;Miller and Troyer, 2002). Of these three properties, biophysical threshold is unlikely to vary systematically with contrast. The resting potential is also unlikely to change: The main stimulus-related influence on resting potential is contrast

adaptation (Carandini and Ferster, 1997;Sanchez-Vives et al., 1997), which should not be a factor here because we randomly interleaved trials of different contrast. Since visual stimuli can have an effect on trial-to-trial variability (Monier et al., 2003), we speculated that contrast-dependent changes in gain might arise from contrast-dependent changes in trial-to-trial variability.

The effects of stimulus contrast on trial-to-trial variability are shown for one cell in Figure 6D–G. Here we refer to a stimulus trial as one complete cycle of the grating, six of which are shown in Fig. 6D for three different stimuli. For the preferred orientation at high contrast (black), the cell responded consistently to each cycle of the grating with a 15–20 mV sinusoidal depolarization, giving rise to a cycle averaged response of similar peak amplitude (Fig. 6E black). To quantify the trial-by-trial variability, we median-filtered the membrane potential to remove spikes, smoothed the traces with a 30-ms sliding window, and then measured the trial-by-trial standard deviation at each point in time relative to the start of the cycle. The standard deviation is indicated in Fig. 6E by gray shading surrounding the black trace, and in this case was relatively small compared to the size of the depolarization. For the preferred stimulus at low contrast (Fig. 6D, blue), the membrane potential response varied considerably from trial to trial: the response was almost as large as the high-contrast response on the 3rd trial, but only a small fraction of that on the 4th trial. As a result, the average peak membrane potential response was about half that evoked by the high-contrast grating (Fig. 6E, blue), yet the standard deviation of the membrane potential was far larger than its high-contrast counterpart (blue shading). This change in response variability is clearly a function of the stimulus and not of the response amplitude: A high-contrast grating at the null orientation (Fig 6D, green) evoked an average response that was comparable in peak amplitude to the low-contrast preferred response, yet had a standard deviation comparable to the high-contrast, preferred response (Fig. 6E, green trace and shading).

The effect of membrane potential trial-to-trial variability on spike rate can be seen in Fig. 6F. At almost every point in time, the low-contrast preferred stimulus evoked a smaller average depolarization than the high-contrast null stimulus (Fig. 6E; green vs. blue), and yet it triggered more spikes because its higher variability more often carried the membrane potential above threshold (Fig. 6F; green vs. blue).

That trial-to-trial variability changes consistently with contrast is shown for this example cell in Fig. 6G. When the peak amplitudes (F1+DC) for all of the individual stimulus trials were plotted against orientation for the cell in Fig. 6D–F, the vertical spread of points was visibly greater at low contrast (compare Fig. 6G, left and right). To quantify the relationship between stimulus contrast and trial-to-trial variability across the population, for each cell we measured the trial-to-trial standard deviation of peak response amplitude at each contrast and orientation. Standard deviation at high contrast is plotted against standard deviation at low contrast for the preferred orientation in Figure 6H, and for the null orientation in Figure 6I. For both orientations, variability was, on average, higher at low contrast (51% more at the preferred and 30% more at the null). That trial-to-trial variability of the peak response amplitude is higher for low-contrast stimuli of other orientations is shown in Supplementary Figure 1. The figure also illustrates, as observed previously (Monier et al., 2003), that the trail-to-trail variability of responses to high-contrast stimuli was reduced relative to the blank stimulus.

The effect of trial-to-trial variability on firing rate

We have proposed that lower contrast leads to larger trial-to-trial variability and that larger variability in turn leads to higher spikes rate. The data in Fig. 6 show that trial-to-trial variability and the membrane-potential-to-spike-rate transformation both depend on contrast, but not that the spike rate transformation depends directly on variability. In order to make this connection, we plotted spike rate against mean membrane potential for different levels of variability (Fig.

7A and B). For each of 36 stimuli (3 contrasts and 13 orientations), responses were divided into 8 epochs of 30-ms duration. Mean potential, standard deviation of mean potential across cycles and mean spike rate were calculated for each epoch. The resulting 312 data points (8 epochs, 36 stimuli) were then grouped into bins of 2.25 mV in mean membrane potential and 0.625 mV of standard deviation, and the corresponding spike rates were averaged. Fig. 7A (which illustrates a different cell than in Fig. 6A and B) indicates that increases in membrane potential variability lead to increases in spike-rate, much the same way that increases in mean membrane potential lead to larger spike-rates. To capture this trend, we applied an extension of the power law (Eq. 1) in which an increase in trial-to-trial variability (standard deviation) was essentially equivalent to an increase in mean potential:

$$R(\overline{V_m},\ std_{V_m}) = k_1\left\lfloor\left(\overline{V_m} - V_{rest}\right) + k_2 * SD_{V_m}\right\rfloor_+^p \quad (2)$$

Where $\overline{V_m}$ is the mean membrane potential averaged across trials, SD_{Vm} is the trial-to-trial standard deviation of the membrane potential, and k_1 and k_2 are constants. The fit of Equation 2 for the cell in Fig. 7A is shown by the smooth curves. In Fig. 7B the data points and fitted curves are replotted against the effective membrane potential, $\left(\overline{V_m} - V_{rest}\right) + 0.68 * SD_{V_m}$. Here, the fitted curves, by construction, superimpose on one another, and the transposed points lie clustered along the fit.

In Fig. 7C, the data from Fig. 7A and B are replotted as a color-map of spike rate against mean and standard deviation of membrane potential. Colored lines show the trajectory of the membrane potential response in mean and in standard deviation over the course of 4 different stimuli (high-contrast preferred, black; high-contrast null, green; low-contrast preferred, blue; blank, red). A second example cell (same cell as in Fig. 6D–G) is shown in Fig. 7D. The relationship between mean potential, standard deviation and spike rate is shown for the whole population in Fig. 7E. For each cell the mean and standard deviation of the membrane potential were normalized to the largest stimulus-evoked depolarization; spike rates were normalized to the largest stimulus-evoked spike rate. The color maps for all 39 cells were then averaged together. The average image shows that the effect of increasing either mean membrane potential or membrane potential standard deviation is to increase spike rate.

To evaluate the effectiveness of Equation 2 in capturing the transformation between membrane potential and spike rate, we fit data from each cell to the equation and then made predictions of peak spike rate from mean membrane potential and membrane potential standard deviation. On average, a change in standard deviation was just over half as effective at increasing spike rate as a similar change in mean (k_2 had a roughly Gaussian distribution, with mean and sigma of 0.64 and 0.29). The predictions for all stimuli and all cells were then compared with the actual recorded spikes rates (Fig. 7F). That the points cluster along the line of slope 1 indicates that Equation 2 captures the membrane potential to spike transformation well.

Accounting for contrast invariance in spike-rate responses of simple cells

The amended power law accounts for why the spiking responses to high-contrast null stimuli are so much lower than the spiking responses to low-contrast preferred stimuli that evoke similar mean depolarizations (Fig. 5A and B). Fig. 7G contains the same data as Fig. 5B (spike response to high-contrast null stimuli plotted against response to low-contrast preferred stimuli) with an expanded y-axis; Fig. 7H shows the predictions of spike rate derived from Equation 2. These predictions accurately reconstructed the differential amplification of spike rate responses to stimuli at high and low contrast.

All of the effects described so far – the mixing of cortical and geniculate excitatory input, early contrast saturation in membrane potential responses, and contrast-dependent trial-to-trial variability – should serve to make orientation tuning of simple cells' spike responses relatively invariant to changes in stimulus contrast. As discussed above, these effects are more important for cells that receive the majority of their excitatory input from the LGN, and thus respond to null oriented stimuli with a significant depolarization. The cell in Fig. 8A–D, for example depolarized approximately 3 mV in response to low-contrast stimuli and 6 mV to high-contrast stimuli at the null orientation (Fig. 8A, −90° and 90°). This cell also exhibited early contrast saturation: By 4% contrast, the membrane potential responses were at least half the size of the 64% responses at all orientations.

The membrane-potential-to-spike-rate transformation for the cell was, as expected, highly nonlinear: Even though the membrane potential response at the null orientation was almost 45% of the size of the preferred response (Fig. 8A and C), the null spike response was zero (B and D). Finally, the cell showed contrast- and orientation-dependent (Monier et al., 2003) changes in the trial-to-trial standard deviation of the membrane potential (Fig. 8E). Spike-rate predictions derived from mean membrane potential and standard deviation of membrane potential produced orientation tuning curves (Fig. 8F) that were very similar to the ones derived from the cell's actual responses (Fig. 8D).

A second example cell with no depolarizing response to null-oriented stimuli is shown in Fig. 8G–M). The cell did show considerable contrast saturation in that the 4% responses were over half as large as the 64% responses. Because of the lack of depolarization evoked by null stimuli, the orientation tuning of the membrane potential was largely contrast invariant, and by virtue of the power law (Equation 2), the spike responses were also invariant but with narrower tuning widths (half-width at half height: 26° for membrane potential vs. 13° for spike rate).

The relationship between tuning width and contrast is summarized for the population in Fig. 9. Here we compare half width at half height (HWHH) of the orientation tuning curves, plotting the width at the lowest contrast tested against the width at 64% contrast. (For a discussion of the relationship between HWHH, tuning and tuning curve offset, see Supplementary Figure 2.) For the membrane potential responses, tuning width in many cells narrowed at low contrast relative to high contrast (Fig. 9A). The narrowing was predicted by the feed-forward model as a result of the untuned DC component of the geniculate input (Fig. 1B, right). The mean difference in HWHH between low and high contrast was 7.3° (Fig. 9D). Tuning widths for the spike responses were far narrower than for membrane potential (median 32° vs. 14.5°; note change in scale between Fig. 9A and 9B–C), and much less dependent on contrast, with a 0.3° narrowing on average between high and low contrast (Fig. 9B and E). There were, however, a small number of cells that did not demonstrate contrast invariance in orientation tuning (Supplementary Figure 3).

Finally, we plot the widths of orientation tuning curves derived from predicted spike rates (Fig. 9C and F). Mean narrowing between predicted high and low-contrast widths (0.78°) was comparable to that seen in recorded spike rate; the distribution of contrast-dependent changes in tuning widths was broader, however, than that observed for the data (compare Fig. 9B and E). Not only were predicted and measured changes in tuning width similar over the population, they were also similar on a cell-by-cell basis, as shown in Supplementary Figure 4.

Discussion

Two views of cortical computation have been proposed to account for the selectivity of sensory neurons. In one view, excitatory afferent input provides a rough sketch of the world, which is then refined and sharpened by lateral or feedback inhibition. In the alternative view, excitatory

afferent input is sufficient, on its own, to account for sensory selectivity. We have studied which of these two viewpoints is most appropriate to describe one feature of cortical simple cells, namely, contrast invariant orientation tuning. A purely linear feed-forward model, incorporating only excitatory input from the LGN, predicts that the width of orientation tuning in simple cells broadens with contrast, breaking contrast invariance. Lateral inhibition, in the form of cross-orientation inhibition, is one mechanism that could restore contrast invariance by antagonizing feed-forward excitation at non-preferred orientations. We find instead that the predicted broadening is suppressed by three independent mechanisms, none of which requires inhibition. First, many simple cells receive only some of their excitatory input from geniculate relay cells (Fig. 3), with the remaining excitatory input originating from other cortical neurons with similar preferred orientations (Chung and Ferster, 1998;Ferster et al., 1996). Second, contrast-dependent changes in the trial-to-trial variability of responses lead to contrast-dependent changes in the transformation between membrane potential and spike rate. Third, membrane potential responses of simple cells saturate at lower contrasts than are predicted by a feed-forward model. We consider each of these mechanisms in turn.

Convergence of cortical and thalamic input

Because relay cells of the LGN are insensitive to orientation and because their firing rate responses are rectified, any feed-forward model based solely on input from relay cells predicts that drifting gratings of the non-preferred (orthogonal) orientation evoke a significant unmodulated rise in membrane potential, equal in size to the mean of the preferred response. Contrary to this prediction, few simple cells had been reported to depolarize or spike in response to orthogonal (null) stimuli, prompting the suggestion that null-evoked excitation from the LGN is suppressed by lateral inhibition in the orientation domain, i.e. cross-orientation inhibition or untuned inhibition (Ferster and Miller, 2000;Sompolinsky and Shapley, 1997). We find here that null-oriented stimuli do evoke a significant depolarization in many simple cells, the magnitude of which is directly proportional to the amount of excitatory input each cell receives from the LGN. In simple cells that receive the majority of their input from the LGN, the depolarization matches the prediction of the feed-forward model; in cells that receive only half of their excitation from the LGN and the rest from other cortical cells, the null-evoked depolarization is half as large as expected from the model. This match is inconsistent with the presence of cross-orientation inhibition: If cross-orientation inhibition were active in cortex, the points in Figure 3D would have consistently fallen below the unity line. In the extreme case of perfect null suppression, for example, all of the points would have fallen along the line Y=0. Our results do not exclude the possibility that simple cells receive untuned inhibition (Heeger, 1992;Tao et al., 2004;Troyer et al., 1998), which would decrease the DC component of the response at all orientations nearly equally. Our results are also consistent with previous evidence that inhibition in simple cells is often tuned to the preferred orientation (Anderson et al., 2000b;Ferster, 1986;Martinez et al., 2005) (though see (Borg-Graham et al., 1998)). The push-pull organization of inhibition at the preferred orientation would have little effect on the peak amplitude of the response.

Contrast-dependent changes in trial-to-trial variability

Although the depolarization evoked by stimuli of the null orientation is on average smaller than what is predicted by the feed-forward model, it is often non-zero, and in many cells can be quite large (Figs 2 and 3). Why, then, do so few simple cells respond with spikes at the null orientation? This failure to respond seems especially paradoxical when low-contrast stimuli at the preferred orientation evoke comparable changes in membrane potential and yet do produce spike responses. The difference lies not in the average response (the membrane potential averaged over multiple trials), but in the trial-to-trial variability of the responses: Because the low-contrast preferred responses vary significantly from trial to trial, the membrane potential regularly rises above threshold. High contrast null responses, however, vary less from trial to

trial and thus cross threshold less often. Note that the trial-to-trial variability for high-contrast, null-oriented stimuli can be even lower than the variability in the absence of a stimulus (Fig. 7C and D). Thus a reduction in variability could be the source of the null-evoked suppression of spontaneous firing that has been observed in some simple cells (Alitto and Usrey, 2004).

In trying to predict the mean spike rate that is evoked by a given stimulus, then, one must consider not only the mean depolarization evoked by the stimulus, but also the response variability (Azouz and Gray, 2000). A rise in either will tend to trigger spikes. Here, we have expressed this relationship as an extension of the power law relationship between mean potential and mean spike rate (Hansel and van Vreeswijk, 2002;Miller and Troyer, 2002), where the mean potential is replaced by the sum of mean and membrane potential variability (Equation 2). We note, however, that this formulation was not derived analytically. It constitutes a convenient extension of the power law that fits the data in a simple way, but the exact form of the equation carries no theoretical significance.

The contrast dependence of trial-to-trial variability that we report here is somewhat larger than was reported previously (Anderson et al., 2000c). We attribute the difference between the two studies to a difference in the way trial-to-trial variability was measured. Anderson et al. averaged variability over the course of an entire grating cycle, whereas we analyzed variability at the peak of the response, where the cells most often fire action potentials. Because variability changes over the course of a cycle (see voltage trajectories in Fig. 7C and D), the two measures are not equivalent.

Saturation

In addition to contrast-dependent changes in trial-to-trial variability, a second aspect of cortical responses that contributes to contrast invariant orientation tuning is the early saturation of simple cell membrane potential responses relative to what is predicted by the feed-forward model. The spiking responses of geniculate relay cells are, on average, only half saturated at 16% or 20% contrast. In the majority of simple cells, however, membrane potential responses at these contrasts are at or near complete saturation. As a result, membrane potential responses at high (64%) and relatively low contrasts (~8%) are more similar to one another than expected. It is important to note, then, that previous studies of invariance were made using contrasts that are generally higher than the half-saturation point (C_{50}) for simple cell membrane potential responses (Alitto and Usrey, 2004;Anderson et al., 2000c;Skottun et al., 1987). Only at contrasts below 8% does contrast invariance in spike-rate responses occasionally break down, in qualitative agreement with feed-forward predictions (Supplementary Figure 3).

There are several mechanisms that could account for early saturation in the membrane potential responses of simple cells. Thalamocortical and cortico-cortical depression (Abbott et al., 1997;Bannister et al., 2002;Boudreau and Ferster, 2005;Carandini et al., 2002;Kayser et al., 2001;Tsodyks and Markram, 1997) could disproportionately reduce the synaptic efficacy of synaptic input from higher contrast stimuli. So would the reductions in driving force on synaptic currents that occur as a result of strong depolarizations. If changes in depression or driving force at the thalamocortical synapse contributed to early saturation, we would expect the C_{50} of simple cell input to be similar at all orientations. If depression at corticocortical synapses contributed, then we would expect C_{50} to change with orientation, and possibly to vary with the %LGN input a cell received.

Conclusions

Contrast-invariance of orientation tuning is one instance of contrast-gain control (Heeger, 1992). Contrast-invariance requires the preservation of orientation tuning width for different contrasts; contrast-gain control requires the preservation of contrast response functions for

different orientations. These requirements are equivalent: if a response to a stimulus of the non-preferred orientation saturated earlier or later in contrast than the response to the preferred orientation, the orientation tuning curves at different contrasts, when normalized, would not superimpose and would not have the same widths. Our results show, then, that gain control is a property intrinsic to the feed-forward inputs to simple cells.

Gain control constitutes a general problem for sensory systems: How to distinguish changes in stimulus attributes from changes in stimulus strength. Both a drop in stimulus strength and a change in stimulus attribute away from the preferred will cause a reduction in the amplitude of a depolarizing response. Changes in trial-to-trial variability provide a mechanism by which to disambiguate these two events, such that a change in stimulus attribute causes a complete loss of spiking responses, whereas a drop in strength does not. In other words, changes in variability allow a cell to modulate the strength of its response without changing its selectivity. This mechanism requires only a spike threshold and stimulus-dependent changes in response variability, and so may be generally applicable to other parts of the visual system and to other sensory modalities. We note, however, that we have measured this effect by comparing different trials in a single cell. If the brain is to rely on such a mechanism in real time, there must be similar (and uncorrelated) variability among the responses of different cells within a given trial. If stimulus-dependent changes in trial-to-trial variability really do contribute to preserving contrast invariance, where do they arise? One possible source is the changes in the excitability of the cortical circuit that underlie transitions between cortical UP and DOWN states (Anderson et al., 2000a;MacLean et al., 2005;Shu et al., 2003). Another possible source, at least at the null orientation, is shunting inhibition (Borg-Graham et al., 1998;Monier et al., 2003). We find no evidence, however, for either cortically-mediated inhibition or excitation at the null orientation, in that the amplitude of the null-evoked depolarization exactly matches the prediction of the feed-forward model when the %LGN Input each cell receives is taken into account (Fig. 3). This result suggests that the trial-to-trial variability of responses evoked by the null orientation may also originate in the LGN. In support of this suggestion, Kara et al. observed significant contrast-dependent changes in trial-to-trial variability (Fano factor) in individual geniculate relay cells (Kara et al., 2000).

Since Hartline described it in the late 1940's (Hartline, 1949), lateral inhibition has been assumed to shape receptive field selectivity in many sensory domains. In visual cortex, however, much of the detailed behavior of simple cells can be captured by a simple feed-forward model lacking lateral inhibition. Many phenomena assumed to arise from visually selective intracortical inhibition can be accounted for by non-specific nonlinearities that occur at several different stages of processing. The sharpness of orientation tuning (Carandini and Ferster, 2000;Volgushev et al., 2000) and direction selectivity (Jagadeesh et al., 1997;Priebe and Ferster, 2005) arise from spike threshold and the so-called iceberg effect. Cross-orientation suppression can be explained by rectification and contrast saturation in geniculate relay cells (Priebe and Ferster, 2006). Here we show that one of the hallmarks of visual cortex, the contrast invariance of orientation tuning, may arise from contrast saturation, spike threshold, and trial-to-trial variability, all of which operate within the local cortical circuit and its thalamic inputs.

Experimental Procedures

Animal preparation

Anesthesia was induced in young adult female cats with intramuscular Ketamine (10 mg/kg) and Acepromazine (0.7 mg/kg), and maintained with intravenous sodium thiopental (10 mg/kg initial, 2 mg/kg/hr maintenance). Paralysis was induced with intravenous vecuronium bromide (0.2 mg/kg/hr). Animals were artificially respirated through a tracheal cannula at a rate to maintain end tidal CO_2 at 4%. To stabilize the brain, the rib cage was suspended from a clamp on the cervical vertebrae and a bilateral pneuothoracotomy was performed. Rectal

temperature was monitored and maintained at 38.3°C by a feedback controlled infrared lamp. EEG and EKG were monitored and rate of anesthesia was adjusted to maintain the regular occurrence of sleep spindles, and to prevent abrupt changes in heart rate. The pupils were dilated with atropine and nictitating membranes retracted with phenylephrine. The corneas were protected with contact lenses with 4-mm artificial pupils. Methods were approved by the Northwestern University Animal Care and Use Committee.

Recording

Patch recordings in current-clamp mode were obtained *in vivo* from area 17 of the visual cortex (within 5° of the representation of the area centralis). Electrodes were introduced through a craniotomy, which was protected by a solution of 3% agar in normal saline. Patch electrodes were filled with standard K^+-gluconate solution containing ATP and pH and calcium buffers as previously described. Signals were low-pass filtered, digitized at 4096 samples/sec and stored by computer using software written in LabVIEW (National Instruments, Austin, TX). Data were analyzed on-line to determine when enough trials had been performed to yield mean responses with low noise. Extracellular recordings were obtained from the cortex and the LGN with lacquer-coated tungsten electrodes. Spikes were detected with a window discriminator and times of occurrence stored by computer (Bak DDS-2). Each neuron's receptive field was initially characterized by its tuning for location, size, orientation and spatial frequency using gratings. Using these preferences the response of the neurons was measured to a 2 or 4 second presentation of drifting gratings which varied in both contrast and orientation for cortical recordings or contrast alone for LGN recordings.

Visual stimulation

Drifting sinusoidal gratings of different orientation and contrast were displayed on a monitor using the Video Toolbox (Pelli, 1997) running in the Matlab environment on a Macintosh computer (Apple Computer, Cupertino, CA). Monitor mean luminance was 20 cd/m^2; refresh rate was 100 frames/sec and spatial resolution was 1024x768 pixels. The screen was placed at a distance of 48 cm from the cat's eyes and focused on the retina using auxillary lenses and direct ophthalmoscopy.

Electrical stimulation

Electrical stimuli were delivered to the cortex through lacquer-coated tungsten electrodes with 200μ exposed tips. Electrodes were placed at a distance of 1 mm or less from the recording electrode and a depth of 400μ from the cortical surface. Stimuli were 200μs duration, electrode negative at an amplitude of 400μA or less. Previous experiments have shown that during the 50 ms following such stimuli, visual stimuli evoke no spikes in the surrounding cortical cells (Chung and Ferster, 1998). At the same time, visual responses of geniculate relay cells are unaffected.

Data analysis

All analyses were performed using custom software written in Matlab (The Mathworks, Natick, MA). For intracellular data, action potential and membrane potential responses were first segregated. Times of the occurrence of action potentials were determined using a simple threshold procedure. Action potentials were then removed from the membrane potential traces using a 5 ms median filter.

The mean and standard deviation of the membrane potential were measured by aligning each response cycle, except the first cycle, binning the responses in 30 ms intervals, and computing the average and standard deviation at each time point.

Orientation Tuning

For almost any sensory stimulus in any modality, there are two independent aspects of tuning. The first is selectivity, the *amount* the response changes over the full range of stimuli, from best to worst. The second is width of tuning, or how rapidly the response falls off as the stimulus moves away from the preferred.

We most often use a Gaussian fit to the orientation tuning curve:

$$R(\theta) = B + A * \exp((\theta - \theta_p)^2 / (2 * \sigma^2)) \quad \text{(Eq. 3)}$$

where R is the response (membrane potential or spike rate), and θ is orientation. This formulation has the advantage that selectivity and tuning width are represented by two different parameters and are independent of one another: the selectivity is represented as null/preferred, or B/(B+A); tuning width is σ. Thus, cells with high selectivity can have either narrow or broad tuning (gray and black in the left graph below). Similarly, cells with low selectivity can have narrow or broad tuning (right graph).

We have shown previously that tuning width of the synaptic input to simple cells is largely dependent on the aspect ratio of the simple cells subfields (Lampl et al., 2001), and is then narrowed by threshold in the transformation to spike output, as had been postulated by many others(DeAngelis et al., 1993a;Palmer and Jones, 1984). In the feed-forward model (for gratings of infinite extent), stimulus selectivity in the synaptic input to simple cells depends only on the level of spontaneous activity in the presynaptic relay cells (Troyer et al., 1998). The lower the spontaneous activity, the lower the selectivity of the simple cell input, because of rectification of the relay cell responses.

Another traditional measure of orientation tuning Half-Width at Half Height (HWHH), where half-height is half the distance between the maximum response and 0 (not the offset, B). HWHH has the advantage of expressing orientation tuning as a single number, but has the disadvantage of depending both on selectivity and tuning width in a complex way. Circular variance, another commonly used measure of tuning, also depends on both selectivity and tuning width.

Contrast-response functions

Contrast response curves were fit using the Naka-Rushton curve ($R = A * C^n/(C^n + C_{50}{}^n)$). The C_{50} indicates the contrast at which a half-maximal response is generated. Fits were made on the peak response (F1+DC) to each cycle of the stimulus (except the first cycle, which was discarded) using the Gauss-Newton method. 95% confidence intervals for parameter estimates were computed from the Jacobian matrix and residuals using the Matlab function nlparci. Specific analyses are presented at the relevant places in the Results.

Power-law fits

Power law fits are based on the individual measurements of mean Vm and mean spike rate in each of the 30-ms epochs of the intracellular records. p and k in Equation 1 (or p, k_1 and k_2 in Equation 2) are adjusted until the summed least squared error between data and power law is minimized, using the Matlab function lsqcurvefit.

Supplementary Material

Refer to Web version on PubMed Central for supplementary material.

Acknowledgements

We thank Kenneth. D. Miller for helpful discussions and Matteo Carandini, Stephen G. Lisberger, Larry Abbott and Wilson S. Geisler for comments on the manuscript. Supported by grants from the National Eye Institute (R01 EY04726) and National Institutes of Mental Health (P20 MH066239).

References

Abbott LF, Varela JA, Sen K, Nelson SB. Synaptic depression and cortical gain control. Science 1997;275:220–224. [PubMed: 8985017]

Alitto HJ, Usrey WM. Influence of contrast on orientation and temporal frequency tuning in ferret primary visual cortex. J Neurophysiol 2004;91:2797–2808. [PubMed: 14762157]

Anderson J, Lampl I, Reichova I, Carandini M, Ferster D. Stimulus dependence of two-state fluctuations of membrane potential in cat visual cortex. Nat Neurosci 2000a;3:617–621. [PubMed: 10816319]

Anderson JS, Carandini M, Ferster D. Orientation tuning of input conductance, excitation, and inhibition in cat primary visual cortex. J Neurophysiol 2000b;84:909–926. [PubMed: 10938316]

Anderson JS, Lampl L, Gillespie D, Ferster D. The contribution of noise to contrast invariance of orientation tuning in cat visual cortex. Science 2000c;290:1968–1971. [PubMed: 11110664]

Azouz R, Gray CM. Dynamic spike threshold reveals a mechanism for synaptic coincidence detection in cortical neurons in vivo. Proc Natl Acad Sci U S A 2000;97:8110–8115. [PubMed: 10859358]

Bannister NJ, Nelson JC, Jack JJ. Excitatory inputs to spiny cells in layers 4 and 6 of cat striate cortex. Philos Trans R Soc Lond B Biol Sci 2002;357:1793–1808. [PubMed: 12626013]

Borg-Graham LJ, Monier C, Fregnac Y. Visual input evokes transient and strong shunting inhibition in visual cortical neurons. Nature 1998;393:369–373. [PubMed: 9620800]

Boudreau CE, Ferster D. Short-term depression in thalamocortical synapses of cat primary visual cortex. J Neurosci 2005;25:7179–7190. [PubMed: 16079400]

Carandini M. Amplification of Trial-to-Trial Response Variability by Neurons in Visual Cortex. PLoS Biol 2004;2:E264. [PubMed: 15328535]

Carandini M, Ferster D. A tonic hyperpolarization underlying contrast adaptation in cat visual cortex [see comments]. Science 1997;276:949–952. [PubMed: 9139658]

Carandini M, Ferster D. Membrane potential and firing rate in cat primary visual cortex. J Neurosci 2000;20:470–484. [PubMed: 10627623]

Carandini M, Heeger DJ, Senn W. A synaptic explanation of suppression in visual cortex. J Neurosci 2002;22:10053–10065. [PubMed: 12427863]

Chance FS, Abbott LF, Reyes AD. Gain modulation from background synaptic input. Neuron 2002;35:773–782. [PubMed: 12194875]

Chung S, Ferster D. Strength and orientation tuning of the thalamic input to simple cells revealed by electrically evoked cortical suppression. Neuron 1998;20:1177–1189. [PubMed: 9655505]

DeAngelis GC, Ohzawa I, Freeman RD. Spatiotemporal organization of simple-cell receptive fields in the cat's striate cortex. I. General characteristics and postnatal development. J Neurophysiol 1993a; 69:1091–1117. [PubMed: 8492151]

DeAngelis GC, Ohzawa I, Freeman RD. Spatiotemporal organization of simple-cell receptive fields in the cat's striate cortex. II. Linearity of temporal and spatial summation. J Neurophysiol 1993b; 69:1118–1135. [PubMed: 8492152]

Ferster D. Orientation selectivity of synaptic potentials in neurons of cat primary visual cortex. J Neurosci 1986;6:1284–1301. [PubMed: 3711980]

Ferster D. Spatially opponent excitation and inhibition in simple cells of the cat visual cortex. J Neurosci 1988;8:1172–1180. [PubMed: 3357015]

Ferster D, Chung S, Wheat H. Orientation selectivity of thalamic input to simple cells of cat visual cortex. Nature 1996;380:249–252. [PubMed: 8637573]

Ferster D, Miller KD. Neural mechanisms of orientation selectivity in the visual cortex. Annu Rev Neurosci 2000;23:441–471. [PubMed: 10845071]

Freeman TC, Durand S, Kiper DC, Carandini M. Suppression without inhibition in visual cortex. Neuron 2002;35:759–771. [PubMed: 12194874]

Hansel D, van Vreeswijk C. How noise contributes to contrast invariance of orientation tuning in cat visual cortex. J Neurosci 2002;22:5118–5128. [PubMed: 12077207]

Hartline HK. Inhibition of activity of visual receptors by illuminating nearby retinal areas in the Limulus eye. Federal Proceedings 1949;8:69.

Heeger DJ. Normalization of cell responses in cat striate cortex. Vis Neurosci 1992;9:181–197. [PubMed: 1504027]

Hirsch JA, Alonso JM, Reid RC, Martinez LM. Synaptic integration in striate cortical simple cells. J Neurosci 1998;18:9517–9528. [PubMed: 9801388]

Hirsch JA, Martinez LM, Pillai C, Alonso JM, Wang Q, Sommer FT. Functionally distinct inhibitory neurons at the first stage of visual cortical processing. Nat Neurosci 2003;6:1300–1308. [PubMed: 14625553]

Hubel DH, Wiesel TN. Receptive fields, binocular interaction and functional architecture in the cat's visual cortex. J Physiol (Lond) 1962;160:106–154. [PubMed: 14449617]

Jagadeesh B, Wheat HS, Kontsevich L, Tyler CW, Ferster D. Direction selectivity of synaptic potentials in simple cells of the cat visual cortex. J Neurophysiol 1997;78:2772–2789. [PubMed: 9356425]

Kara P, Reinagel P, Reid RC. Low response variability in simultaneously recorded retinal, thalamic, and cortical neurons. Neuron 2000;27:635–646. [PubMed: 11055444]

Kayser A, Priebe NJ, Miller KD. Contrast-dependent nonlinearities arise locally in a model of contrast-invariant orientation tuning. J Neurophysiol 2001;85:2130–2149. [PubMed: 11353028]

Lampl L, Anderson JS, Gillespie D, Ferster D. Prediction of orientation selectivity from receptive field architecture in simple cells of cat visual cortex. Neuron 2001;30:263–274. [PubMed: 11343660]

Lauritzen TZ, Miller KD. Different roles for simple-cell and complex-cell inhibition in V1. J Neurosci 2003;23:10201–10213. [PubMed: 14614078]

Li B, Thompson JK, Duong T, Peterson MR, Freeman RD. Origins of cross-orientation suppression in the visual cortex. J Neurophysiol 2006;96:1755–1764. [PubMed: 16855109]

MacLean JN, Watson BO, Aaron GB, Yuste R. Internal dynamics determine the cortical response to thalamic stimulation. Neuron 2005;48:811–823. [PubMed: 16337918]

Martinez LM, Alonso JM, Reid RC, Hirsch JA. Laminar processing of stimulus orientation in cat visual cortex. J Physiol 2002;540:321–333. [PubMed: 11927690]

Martinez LM, Wang Q, Reid RC, Pillai C, Alonso JM, Sommer FT, Hirsch JA. Receptive field structure varies with layer in the primary visual cortex. Nat Neurosci 2005;8:372–379. [PubMed: 15711543]

McLaughlin D, Shapley R, Shelley M. Large-scale modeling of the primary visual cortex: influence of cortical architecture upon neuronal response. J Physiol Paris 2003;97:237–252. [PubMed: 14766144]

Miller KD. A model for the development of simple cell receptive fields and the ordered arrangement of orientation columns through activity-dependent competition between ON- and OFF-center inputs. J Neurosci 1994;14:409–441. [PubMed: 8283248]

Miller KD, Troyer TW. Neural noise can explain expansive, power-law nonlinearities in neural response functions. J Neurophysiol 2002;87:653–659. [PubMed: 11826034]

Monier C, Chavane F, Baudot P, Graham LJ, Fregnac Y. Orientation and direction selectivity of synaptic inputs in visual cortical neurons: a diversity of combinations produces spike tuning. Neuron 2003;37:663–680. [PubMed: 12597863]

Movshon JA, Thompson ID, Tolhurst DJ. Spatial summation in the receptive fields of simple cells in the cat's striate cortex. Journal of Physiology (London) 1978;283:53–77. [PubMed: 722589]

Palmer LA, Jones JP. Quantitative analysis of cat simple receptive fields in two spatial and two temporal frequency dimensions. Soc Neurosci Abstr 1984;10:800.

Pelli DG. The VideoToolbox software for visual psychophysics: transforming numbers into movies. Spat Vis 1997;10:437–442. [PubMed: 9176953]

Priebe NJ, Ferster D. Direction selectivity of excitation and inhibition in simple cells of the cat primary visual cortex. Neuron 2005;45:133–145. [PubMed: 15629708]

Priebe NJ, Ferster D. Mechanisms underlying cross-orientation suppression in cat visual cortex. Nat Neurosci 2006;9:552–561. [PubMed: 16520737]

Priebe NJ, Mechler F, Carandini M, Ferster D. The contribution of spike threshold to the dichotomy of cortical simple and complex cells. Nat Neurosci. 2004

Reid RC, Alonso JM. Specificity of monosynaptic connections from thalamus to visual cortex. Nature 1995;378:281–284. [PubMed: 7477347]

Sanchez-Vives MV, Nowak LG, McCormick DA. Cellular and network mechanisms generating adaptation to contrast in the visual cortex: An in vivo and in vitro study. Soc Neurosci Abs 1997;23:1944.

Shu Y, Hasenstaub A, McCormick DA. Turning on and off recurrent balanced cortical activity. Nature 2003;423:288–293. [PubMed: 12748642]

Skottun BC, Bradley A, Sclar G, Ohzawa I, Freeman R. The effects of contrast on visual orientation and spatial frequency discrimination: a comparison of single cells and behavior. J Neurophysiol 1987;57:773–786. [PubMed: 3559701]

Somers DC, Nelson SB, Sur M. An emergent model of orientation selectivity in cat visual cortical simple cells. J Neurosci 1995;15:5448–5465. [PubMed: 7643194]

Sompolinsky H, Golomb D, Kleinfeld D. Global processing of visual stimuli in a neural network of coupled oscillators. PNAS 1990;87:7200–7204. [PubMed: 2402502]

Sompolinsky H, Shapley R. New perspectives on the mechanisms for orientation selectivity. Current Opinion in Neurobiology 1997;7:514–522. [PubMed: 9287203]

Stratford KJ, Tarczy HK, Martin KA, Bannister NJ, Jack JJ. Excitatory synaptic inputs to spiny stellate cells in cat visual cortex. Nature 1996;382:258–261. [PubMed: 8717041]

Tao L, Shelley M, McLaughlin D, Shapley R. An egalitarian network model for the emergence of simple and complex cells in visual cortex. Proc Natl Acad Sci U S A 2004;101:366–371. [PubMed: 14695891]

Tolhurst DJ, Heeger DJ. Comparison of contrast-normalization and threshold models of the responses of simple cells in cat striate cortex. Vis Neurosci 1997;14:293–309. [PubMed: 9147482]

Troyer TW, Krukowski AE, Priebe NJ, Miller KD. Contrast-invariant orientation tuning in cat visual cortex: thalamocortical input tuning and correlation-based intracortical connectivity. J Neurosci 1998;18:5908–5927. [PubMed: 9671678]

Tsodyks MV, Markram H. The neural code between neocortical pyramidal neurons depends on neurotransmitter release probability [published erratum appears in Proc Natl Acad Sci U S A 1997 May 13;94(10):5495]. Proc Natl Acad Sci U S A 1997;94:719–723. [PubMed: 9012851]

Volgushev M, Pernberg J, Eysel UT. Comparison of the selectivity of postsynaptic potentials and spike responses in cat visual cortex. Eur J Neurosci 2000;12:257–263. [PubMed: 10651880]

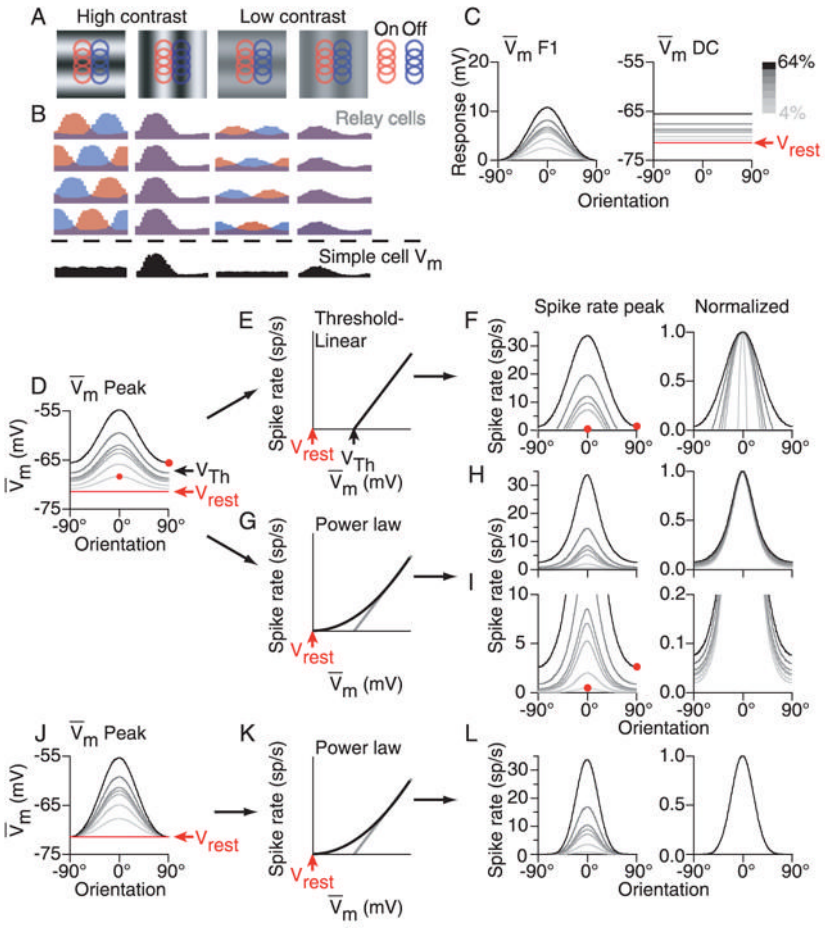

Figure 1.

Contrast dependence of orientation tuning in a feed-forward model of simple cells. **A**. Receptive fields and responses (colored traces) for 8 of the 16 relay-cell inputs to the model simple cell. **B.** Responses to both preferred and null-oriented gratings at high and low contrast are shown, as is the total input (black traces). **C**. Orientation tuning curves for the F1 and DC components of the synaptic input to the simple cell. **D**. Orientation tuning curve of the peak input to the simple cell (F1+DC). **E.** A threshold-linear transformation between membrane potential and spike rate. **F.** Orientation tuning curves (raw values and normalized) for peak spike rate as predicted by the threshold-linear transformation. **G**. A power-law transformation between membrane potential and spike rate. **H**. Same as E for the power-law transformation. **I**. Same as G with amplified vertical scale. **J–L**. Same as C, F and G with the DC component of the membrane potential response removed.

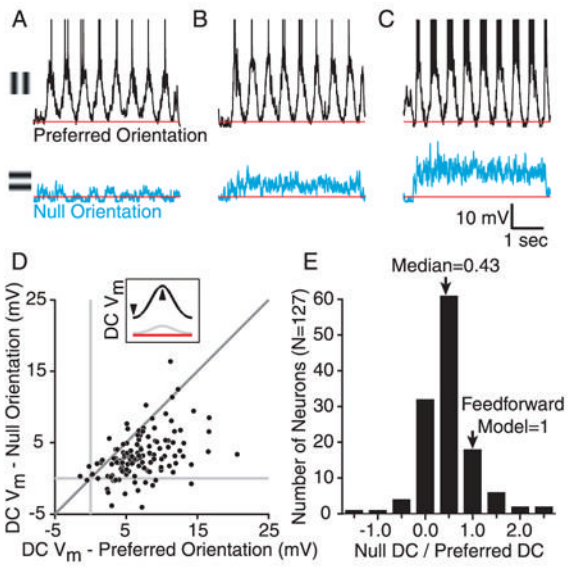

Figure 2.

Responses of simple cells to gratings of the preferred and orthogonal orientation. **A–C**. 8 cycles of response to a high-contrast drifting grating at the preferred (above) and orthogonal or null orientation (below) for three cells. Grating onset occurred after 250ms of blank stimulation. **D**. The DC components of the responses to high-contrast gratings of the preferred and null orientation plotted against one another for 127 cells. **E**. A histogram of ratios for the values in D.

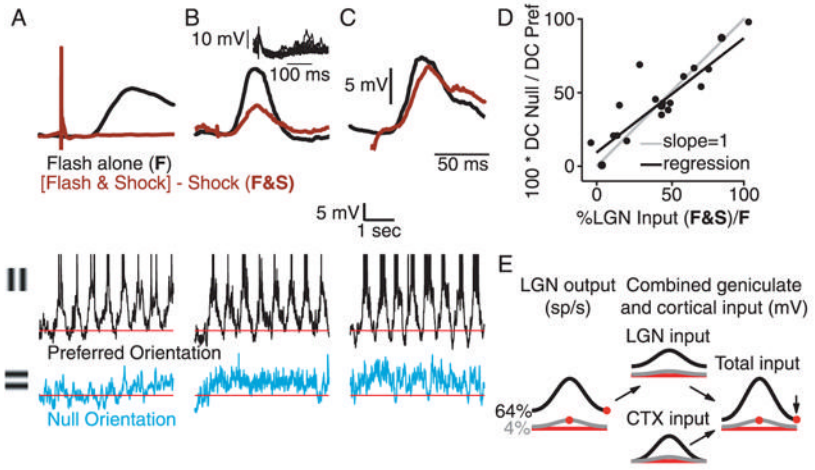

Figure 3.

The relationship between the response to null-oriented stimuli and the amount of input from the LGN. **A–C**. Top, responses to optimal flashed gratings with (brown) and without (black) paired electrical stimulation of nearby cortex for 3 cells. The response to electrical stimulation alone has been subtracted from the brown traces. The ratio of the amplitudes of the brown and black traces (F&S/F) is taken to be the proportion of synaptic input the cell receives directly from the LGN. The cell in A receives almost no direct input from the LGN; the cell in C receives almost exclusive input from the LGN. Middle and bottom, responses to high-contrast drifting gratings of the preferred and null orientation for the 3 cells. Inset in B shows 20 superimposed responses to electrical stimulation alone. **D.** The ratio of responses to null and preferred stimuli (DC component) plotted against the proportion of input provided by the LGN (N=19). **E**. Left, orientation tuning curves for the combined output from the relay cells exciting the model simple cell that receives input only from the LGN. Right, orientation tuning curves for a cell that receives half it's input from the LGN and half from other cortical cells with similar preferred orientation. The main effect is to reduce the response of the cell to stimuli of the null orientation.

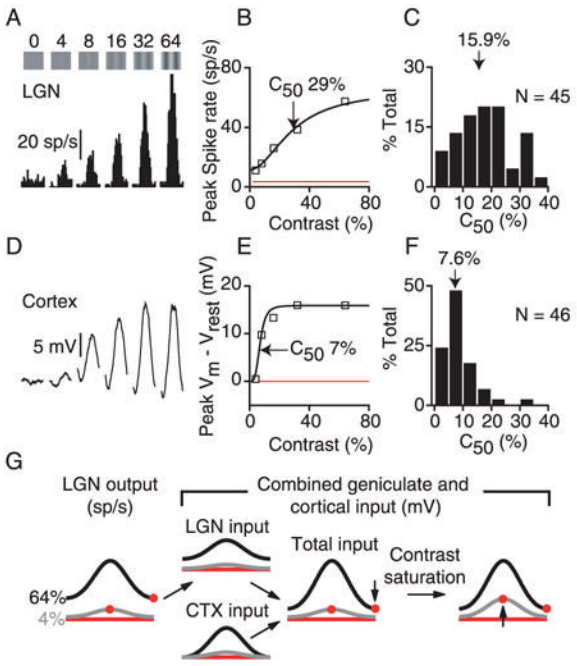

Figure 4.

Contrast saturation in LGN and cortex. **A**. Spike responses of a geniculate relay cell to drifting gratings of different contrast. **B**. Contrast response curve constructed from the peak (F1+DC) responses in A. **C**. A histogram of C_{50}'s for 45 relay cells. **D–F**. Same as A–C for the peak membrane potential responses of 46 cortical simple cells. **G**. Same as Fig. 3E, but with the addition of early contrast saturation. The effect of early saturation is to raise the amplitude of responses to low-contrast stimuli of the preferred orientation.

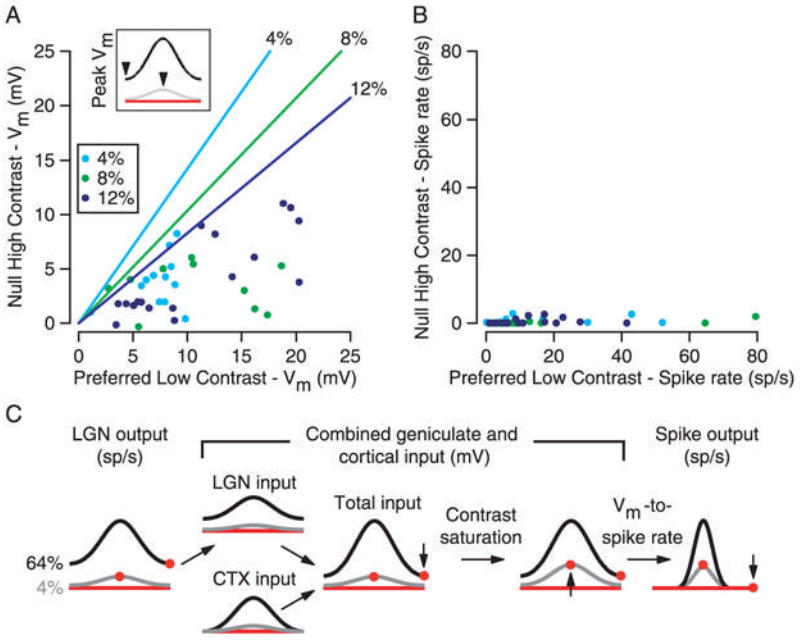

Figure 5.

Lack of spiking responses to high-contrast stimuli of the null orientation. **A** and **B**. The response (A - membrane potential; B - spike rate) to high-contrast stimuli of the null orientation plotted against the response to low-contrast stimuli of the preferred orientation. Symbols of different shades of gray indicate the contrast of the low-contrast stimulus. Lines indicate the predictions of the feed-forward model in Fig. 1. **C**. Same Figs. as 3E and 4G, with the addition of the V_m-to-spike-rate transformation, which differentially amplifies the responses to high-contrast preferred and low-contrast null stimuli while narrowing the tuning curves equally.

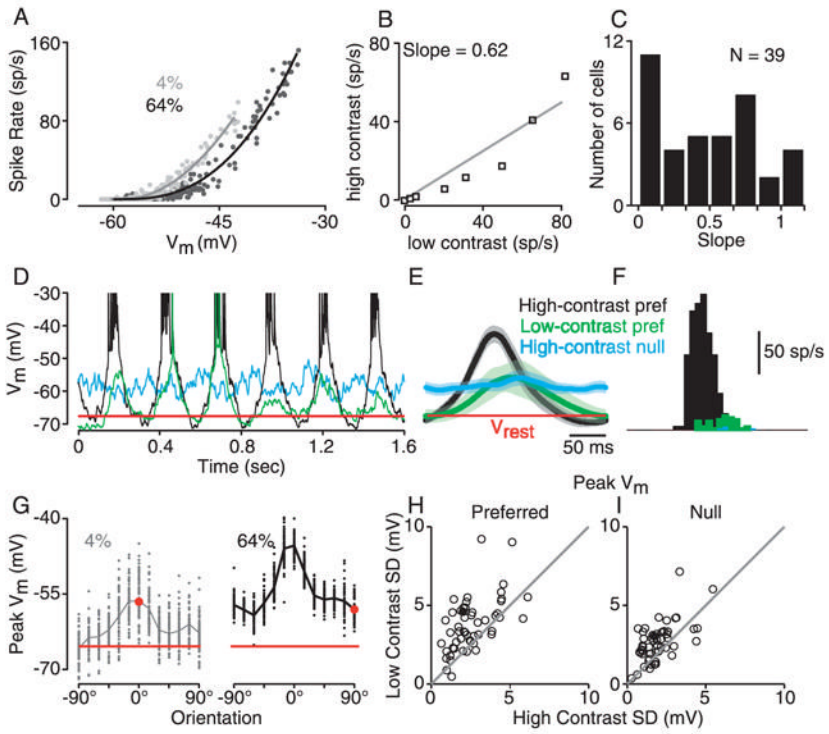

Figure 6.

The contrast dependence of trial-to-trial variability and its effect on mean spike rate. **A**. The relationship between mean spike rate and mean membrane potential plotted separately for low-contrast and high-contrast stimuli in one simple cell. Each point is derived from one 30-ms epoch of a trial-averaged response (13 stimuli, 16 epochs each). Solid curves are power-law fits (Equation 1) to the data. **B**. Average spike rate at high contrast plotted against spike rate at low contrast for each of 8 ranges of mean membrane potential in A. Solid line is a linear regression. **C**. Slope of the regression (as in B) for 39 cells. **D**. Six cycles of the responses of a simple cell to high- and low-contrast gratings of the preferred orientation (black and blue) and to a low-contrast grating of the null orientation (green). **E**. Cycle-averages of the responses to the three stimuli, with standard deviation indicated by shading. The mean and standard deviation of the membrane potential were computed using a 30 ms sliding window. **F**. Average spike responses for the three stimuli. **G**. Orientation tuning curves for the peak (F1+DC) response of the cell at high and low contrast. Each point represents the peak response to a single cycle. **H**. The trial-to-trial standard deviation of peak response amplitudes for low-contrast gratings plotted against the standard deviation for high-contrast gratings at the preferred and null orientations (52 cells).

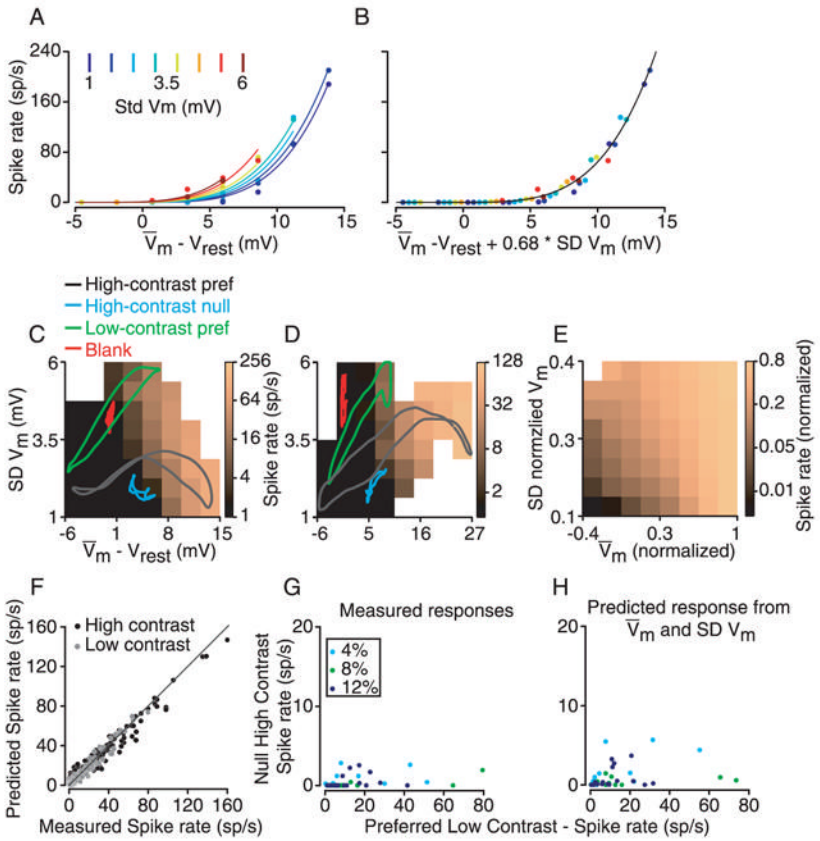

Figure 7.

The relationship between membrane potential mean, standard deviation, and spike rate. **A**. Mean and standard deviation of membrane potential and mean spike rate were measured in 30-ms epochs taken from the responses to gratings of different orientations and contrast. Data were binned into 2.25-mV intervals of mean potential and 0.625-mV intervals of standard deviation (SD) and then mean spike rate was plotted against mean membrane potential for 8 different SD intervals as indicated by the color legend. Curves are a fit to Equation 2. **B**. Same data as in A, with spike rate plotted against mean membrane potential plus 0.68 times SD. **C**. Same data as in A and B plotted as a color-map of spike rate against mean and standard deviation of membrane potential. Colored lines indicate the trajectory of mean and SD of membrane potential evoked by 4 different stimuli over the course of one grating cycle (high-contrast preferred, black; high-contrast null, blue; low-contrast preferred, green; blank, red). The mean and standard deviation of the membrane potential were computed using a 30 ms sliding window. **D**. Same as C for the cell from Fig. 6D–G. **E**. Same as C and D averaged over 39 cells. V_m and SD-V_m are normalized for each cell to the amplitude of the largest membrane potential response. **F**. For 39 cells, the spike responses to stimuli of all orientations at high and low contrasts were calculated from Equation 2 using the corresponding membrane potential responses. The predicted spike rates are plotted against measured spike rates for each stimulus. **G**. Data from Fig. 5B (spike-rate responses to high-contrast null and low-contrast preferred stimuli plotted against one another) replotted with a magnified y-scale. **H**. Same as G, except that the spike rates plotted are predicted from membrane potential using Equation 2.

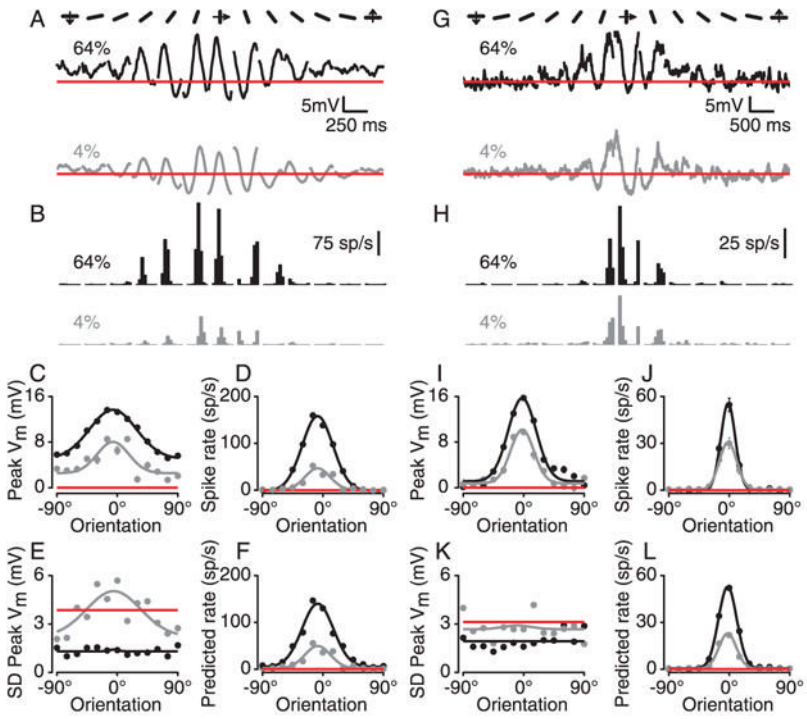

Figure 8.

Contrast invariance of orientation tuning in two simple cells. **A**. Cycle-averaged membrane potential responses to gratings of high and low contrast and different orientations. **B**. Corresponding spike responses. **C–G**. Orientation tuning curves at high and low contrast for mean membrane potential, spike rate, standard deviation of membrane potential and predicted spike rate (from Equation 2). **G**–**M**. Same as A–F for a second cell.

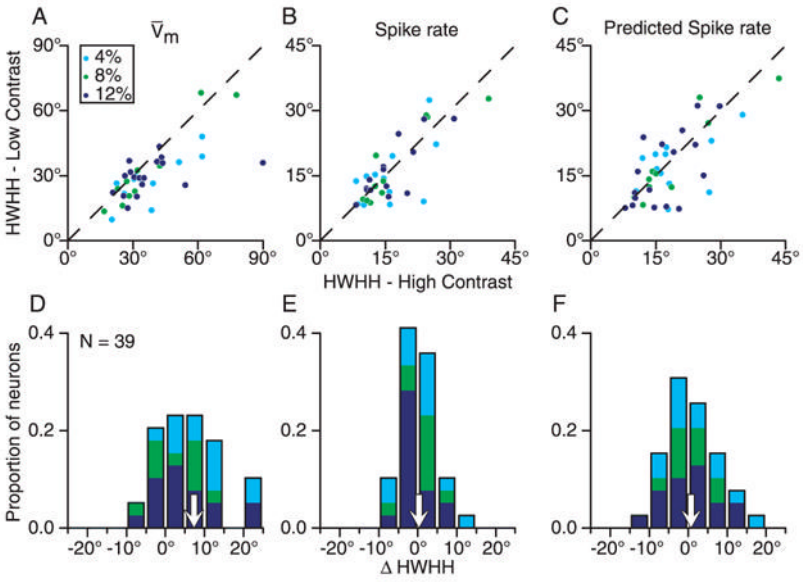

Figure 9.

Contrast dependence of orientation tuning width. **A**–**C**. Half-width at half height (HWHH) of the orientation tuning curves at high and low contrast compared for mean membrane potential, measured spike rate, and spike rate predicted from Equation 2. **D–F**. Histograms of low-contrast HWHH minus high-contrast HWHH.